An easy to implement strategy for improving organic electrochemical transistor stability: Combining chemical doping with solvent degassing.

Alexandra Paterson

alexandra.paterson@uky.edu

The University of Kentucky https://orcid.org/0000-0002-8395-308X

Vianna Le

University of Kentucky

Kyle N. Baustert Kyle N. Baustert

University of Kentucky

Megan Brown

University of Kentucky

Joel Bombile

University of Kentucky

Lucas Flagg

NIST

Karl Thorley

University of Kentucky

Christina Kousseff

University of Oxford

Olga Solomeshch

Technion

Iain McCulloch

Princeton

Nir Tessler

Technion

Chad Risko

University of Kentucky

Kenneth Graham

University of Kentucky

Article

Keywords: organic electrochemical transistors, chemical doping, organic mixed ionic electronic conductors, stability, threshold voltage

Posted Date: April 15th, 2024

DOI: https://doi.org/10.21203/rs.3.rs-4224356/v1

Additional Declarations: There is **NO** Competing Interest.

An easy to implement strategy for improving organic electrochemical transistor stability: Combining chemical doping with solvent degassing

*Vianna N. Le, Kyle N. Baustert, Megan Brown, Joel H. Bombile, Lucas Q. Flagg, Karl Thorley, Christina J. Kousseff, Olga Solomeshch, Iain McCulloch, Nir Tessler, Chad Risko, Kenneth R. Graham, Alexandra F. Paterson**

V. N. Le, Prof. A. F. Paterson
Department of Chemical and Materials Engineering, Department of Electrical Engineering, Centre for Applied Energy Research
University of Kentucky, Lexington, Kentucky 40506, USA
E-mail: alexandra.paterson@uky.edu

K. N. Baustert, Prof. K. R. Graham
Department of Chemistry, University of Kentucky, Lexington, Kentucky 40506, USA

Dr. O. Solomeshch, Prof. N. Tessler
Sara and Moshe Zisapel Nano-Electronic Center
Department of Electrical Engineering
Technion - Israel Institute of Technology
Haifa 3200, Israel

M. Brown, Dr. J. H. Bombile, Prof. C. Risko
Department of Chemistry, and Centre for Applied Energy Research, University of Kentucky, Lexington, Kentucky 40506, USA

Dr. K. Thorley
Department of Chemistry, and Centre for Applied Energy Research, University of Kentucky, Lexington, Kentucky 40506, USA

Lucas Q. Flagg
Materials Science and Engineering Division
National Institute of Standards and Technology
Gaithersburg, Maryland 20899, USA

Dr. C. J. Kousseff, Prof. I. McCulloch
Department of Chemistry, Chemistry Research Laboratory, University of Oxford, Oxford, OX1 3TA, UK

Keywords: organic electrochemical transistors; chemical doping, organic mixed ionic electronic conductors; stability; threshold voltage

Although p-type organic mixed ionic electronic conductors (OMIECs) are susceptible to oxidation, it has not yet been considered as to whether oxygen could behave as an uncontrolled p-dopant. Here, oxygen dissolved in solvents is shown to be behave as a p-dopant, that fills traps to enable more effective electrochemical doping in OMIECs and organic electrochemical transistors (OECTs). Yet the presence of oxygen also jeopardizes OECT stability. A two-step strategy is introduced to solve this contradictory problem, where first the solvent is degassed, and second the OMIEC is doped in a controlled manner using a chemical dopant. This strategy increases on-off ratio, tunes the threshold voltage, and enhancing the transconductance, mobility and the μC* product, while having a remarkable impact on both p-type and n-type OECT stability in air and water. This simple solution-processing technique is easily implemented, low-cost, and highly effective in air and water. The data herein suggests that combining chemical doping with solvent degassing could be a broadly applicable technique to improve essential criteria needed to realize organic bioelectronics and more complex OMIEC circuitry.

Organic mixed ionic-electronic conductors (OMIECs) and organic electrochemical transistors (OECTs), which simultaneously couple and transport ionic and electronic charges, are attracting interest for an enormous application space: From biosensors,[1,2,3,4,5] medical devices and drug delivery,[6,7] adaptive healthcare technologies,[6,7,8] and body-machine interfaces,[9] to artificial synapses for coupling neurons and controlling prosthetic devices,[10] neuromorphic hardware and computing,[11,12,13,14,15] chemical sensing[16,13,17,18] and agricultural applications.[19,20] OECT research has made significant progress in recent years.[21, 22, 23, 24, 25] However, high on-off current ratios

($I_{ON/OFF}$) and tunable threshold voltages (V_T) are remaining bottlenecks to for realizing more complex bioelectronic circuitry.[26,27] Additionally, poor operational stability is a major concern for OECTs.[26] While stability is a universal requirement for all transistors, OECTs have a unique challenge in that they must be stable in air and in water-based electrolytes.[28, 29, 30, 31,32, 33, 34]

Improving OECT stability in air and water is not straightforward. Oxygen (O_2) plays a crucial, detrimental role in OECT stability, and O_2 is abundantly present in OECTs that operate in air and water. The redox potential of O_2 is close to redox active OMIEC oxidation potentials[35] and, depending on the quantity of dissolved O_2, the OMIEC and the voltage applied,[36, 37, 38, 39] O_2 can lead to parasitic side reactions that form hydrogen peroxide (H_2O_2) or hydroxide (OH^-) [29, 40] – both of which have been shown to reduce operational stability in OECTs.[35, 41, 42] Redox reactions between O_2 dissolved in NaCl electrolyte and degrade glycolated polythiophene OECT by increasing the pH and presence of OH^-, and lower the performance of PEDOT:PSS OECTs.[42,39] Additionally, Faradaic reactions with O_2 can corrode the host OMIEC,[35] cause reactions that are detrimental to biosensors such as lipid peroxidation,[43, 44, 45] ORR side reaction products H_2O_2 and OH^- impact sensing efficiency and can be toxic to biological environments;[46, 47] and O_2 has been shown to reduce PEDOT:PSS OECT capacitance and current.[41]

While O_2 and/or its subsequent compounds clearly threaten OMIEC stability, there is a significant body of literature showing that O_2 can behave as a p-dopant to enhance performance in low ionization energy (IE) organic electronic materials.[48,49,50,51,52] Although easy oxidation is a key design principle for p-type OMIEC,[53,54] it has not yet been considered as to whether O_2 behaves as p-dopant in OECTs. Here, we show using ultraviolet photoelectron spectroscopy (UPS),

electron paramagnetic resonance (EPR) and density functional theory (DFT) that O_2 dissolved in solvents acts as a p-dopant in p-type OMIECs. OECTs suggest O_2 p-doping fills traps to enable more effective electrochemical doping – yet O_2 also jeopardizes OECT stability. A new, two-step materials engineering strategy is introduced to solve the problem arising from this contradiction. First, solvents are degassed using a freeze-pump-thaw method. Second, a chemical dopant is introduced into the OMIEC. This two-step strategy simultaneously tunes V_T, improves $I_{ON/OFF}$, and enhances the μC^* product, while realizing, to the best of our knowledge, the most stable p-type and n-type OECTs in air and water to-date, and highest $I_{ON/OFF}$ ratios to-date for a planar OECT. UPS, EPR, ultraviolet-visible absorbance (UV-Vis), atomic force microscopy (AFM) and grazing-Incidence wide-angle X-ray scattering (GIWAXS) show p-doping mechanisms work synergistically with morphology changes to enhance OECT performance metrics. The two-step technique is shown to be effective for different polymers, solvent and dopants. Overall, the work reported here suggests that combining chemical doping with degassed solvents is a highly effective, low-cost, easy to implement technique that broadly impacts criteria needed to realize more complex OMIEC, OECT, and organic bioelectronic circuitry.

O_2 p-doping is well-known in organic electronics – from published findings,[50, 55, 56 48,49 50,51,52] to anecdotal strategies on leaving p-type organic devices outside the glovebox. O_2 is present in dissolved quantities in solvents exposed to air, such as chloroform (CF). CF is routinely used to process OMIECs from solution,[57,58, 59, 60] because OMIECs are highly soluble in CF, it is low-cost, and has lower toxicity relative to other organic electronic solvents, including chlorobenzene and tetralin[61, 62, 63]. We degassed CF using a freeze-pump-thaw method to explore whether O_2 dissolved in CF acts as a p-dopant, in representative p-type polyethylene glycol functionalized

OMIEC, p(g3T2),[64,65, 66] with ionization energy (IE) of 4.46 eV (**Figure 1b**).[66] **Figure 1 c-d** compares p(g3T2) processed from degassed-CF with p(g3T2) processed from CF stored in air (i.e.,, ambient-CF) using UPS. UPS indicates that, unless CF is degassed, p(g3T2) is p-doped. Specifically, the work function shifts from 4.0 eV for the degassed-CF p(g3T2), to 4.3 eV for the p(g3T2) ambient-CF, and p(g3T2) has larger IE (4.6 eV) when processed using ambient-CF compared to degassed-CF (4.3 eV).[67] To confirm O_2 is the primary p-dopant, rather than other volatile species removed during degassing, we used density functional theory (DFT) and an oxygen sensor. DFT (**Figure S1** and **Figure S2**) indicates the thermodynamics are highly favourable for O_2 to behave as the primary p-dopant, and that chlorine gas and trichloroacetic acid may possibly oxidize p(g3T2), based on the proximity of their electron affinity (EA) to the p(g3T2) IE. Next, the 5,11-bis(triethylsilylethynyl)anthradithiophene (TES-ADT) oxygen sensor in **Figure S3** shows O_2 is present in the ambient-CF, but not present in the degassed-CF.[68] In addition to degassed-CF and ambient-CF coming from the same non-anhydrous bottle stored in air (see Experimental Section), the fact that degassing is widely employed to remove O_2 from solvents in organic reactions, and that O_2 is more likely to behave as an oxidant in the presence of acids such as hydrochloric acid,[69] we attribute the UPS data to O_2 dissolved in CF acting as primary p-dopant in p(g3T2).

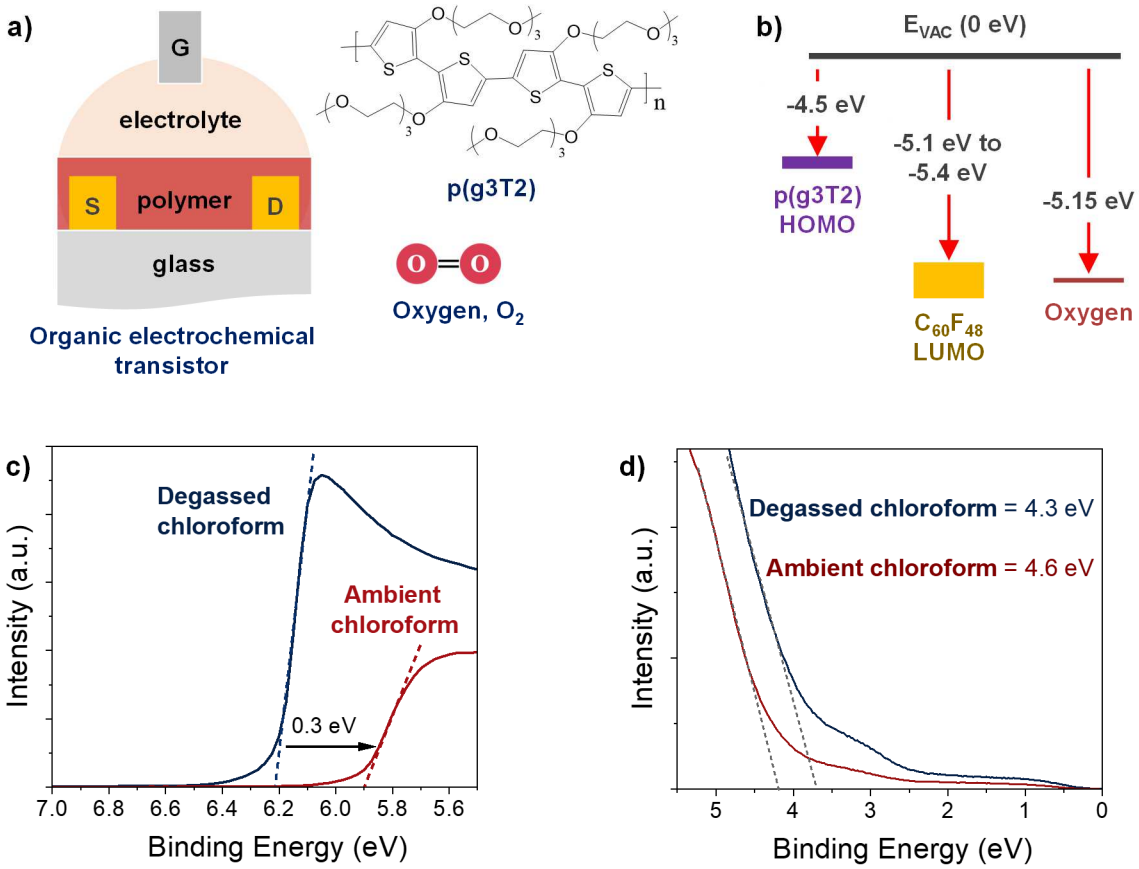

Figure 1. Oxygen dissolved in solvents is an uncontrolled p-dopant in organic mixed conductors. (a) An organic electrochemical transistor (OECT) schematic with chemical structure of p(g3T2) and oxygen (O_2). (b) Energy level diagram for p(g3T2), O_2 and $C_{60}F_{48}$. (c) Ultraviolet photoelectron spectroscopy (UPS) data showing the secondary electron cut-off region of p(g3T2) thin-films prepared with degassed-chloroform and ambient-chloroform ($h\nu$ = 10.2 eV). The shift in the work function (WF) by 0.3 eV indicates that if the chloroform is not degassed, then it will p-dope the OMIEC. The WF of the p(g3T2) prepared from degassed-chloroform is 4.0 eV, compared to the ambient-chloroform WF of 4.3 eV. (d) UPS HOMO onset region.

Because doping plays an important role in transistor performance, we explored the impact of O_2 p-doping on p(g3T2) OECTs. OECTs were measured in a nitrogen glovebox using an ionic liquid, 1-butyl-3-methylimidazolium tetrafluoroborate, [BMIM][BF_4], as the electrolyte, to avoid introducing other sources of O_2 and focus only on the impact of removing O_2 from the solvent.

The most extreme case is shown in **Figure 2a-b** and **Figure S4a-b**. Degassed-CF reduces the on-current (I_{ON}) by three orders of magnitude, the off-current (I_{OFF}) by two orders of magnitude, and the corresponding transconductance (g_m) for the transistors in **Figure 2** reduces from 1.6 mS to 0.18 mS. **Figure S1c** shows the cyclic voltammetry (CV) curves and OECT output curves, respectively. However, **Figure S1d** indicates that, while ambient-CF outperforms degassed-CF, statistically across 6 OECTs, charge carrier mobility (μ) values are not remarkably dissimilar. One possibility is O_2 p-doping fills trap states rather than improves performance metrics,[48] which may enable more effective electrochemical doping with gate voltage (V_G). To approach the challenge of retaining trap filling effects, while enhancing OECT performance and removing O_2 that causes stability, we identified a chemical p-dopant. We chose the fluorinated fullerene, $C_{60}F_{48}$ (**Figure 2c**), because it is an effective p-dopant,[70, 71, 72,73] has favorable energetics for p(g3T2) (**Figure 1b**), and once it has reacted to p-dope the host OMIEC, it is unlikely to impart additional chemistry to the polymer. **Figure 2d** shows the results for degassed-CF:$C_{60}F_{48}$ OECTs at 100 molar weight percentage (mol%), i.e. degassed-CF:$C_{60}F_{48}$(100 mol%); there is a substantial, four orders of magnitude increase in I_{ON}, and a remarkable maximum $I_{ON/OFF} \approx 1.4 \times 10^6$, with an average $I_{ON/OFF} \approx 3.3 \times 10^5$ over six OECTs. The maximum $I_{ON/OFF}$ value is one of the highest reported values for a planar OECT to-date.[74]. In the most extreme case (i.e., transistors in **Figure 2b** and **Figure 2d**), g_m increases by over 100 ×, from 0.18 mS to 25.1 mS. To quantify the μC^* product, the volumetric capacitance (C^*) was measured by fitting electrochemical impedance spectroscopy (EIS) data (**Figure S5**). **Table 1** and **Figure S6** further supports of the remarkable impact that chemical p-doping combined with solvent-degassing has on OECT figures of merit, with the average μC^* product extracted from g_m for six OECTs per system being 113 F/cmVs, 93 F/cmVs, and 680 F/cmVs for ambient-CF, degassed-CF and degassed-CF:$C_{60}F_{48}$, respectively. OECT data indicates

adjusting the concentration of chemical p-dopant is an excellent technique to control V_T. Specifically, **Figure S6c** shows V_T shifts towards 0 V, from average values of -0.13 V to -0.08 V, in the degassed-CF and degassed-CF:$C_{60}F_{48}$ OECTs, respectively, that is characteristic of doped transistors.[75] Overall, chemical doping clearly has a significant impact on OECT performance metrics.

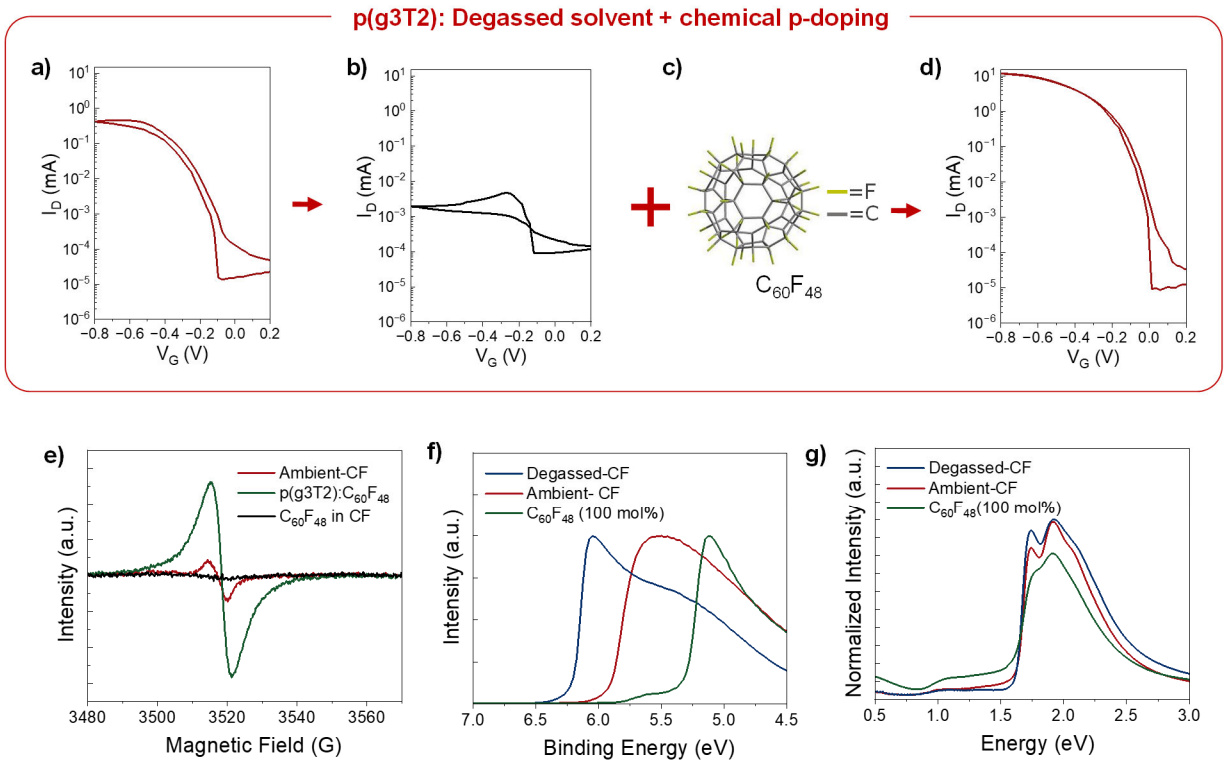

Figure 2. The impact of solvent degassing and chemical p-doping on organic electrochemical transistors. Representative p(g3T2) OECT transer curves measured at V_D = -0.6 V, for solutions prepared with (a) ambient-CF and (b) degassed-CF. (c) The chemical structure of the chemical p-dopant, the fluorinated fullerene $C_{60}F_{48}$. (d) Representative p(g3T2) OECT transfer curves measured at V_D = -0.6 V, for a solution prepared with degassed-CF:$C_{60}F_{48}$(100 mol%). OECTs were tested at 0.52 V/s scan rate with a [BMIM][BF_4] electrolyte, in a nitrogen filled glovebox, to remove O_2 and focus the study only on O_2 p-doping occurring because of dissolved O_2 in ambient-CF. (e) Room temperature electron paramagnetic resonance (EPR) comparing 5 mg/mL p(g3T2)

solutions prepared from ambient-CF and degassed-CF:$C_{60}F_{48}$(100 mol%), indicating that $C_{60}F_{48}$ is a more effective p-dopant than O_2. Data for pristine $C_{60}F_{48}$ is also shown. (f) Ultraviolet photoelectron spectroscopy (UPS) comparing p(g3T2) thin-films made from solutions prepared with degassed-CF, ambient-CF, and degassed-CF:$C_{60}F_{48}$(100 mol%). (c) Ultraviolet–visible (UV-Vis) absorption comparing p(g3T2) thin films processed from degassed-CF, ambient-CF, and degassed-CF:$C_{60}F_{48}$(100 mol%).

EPR, UPS and ultraviolet-visible absorbance (UV-Vis) were used to confirm that $C_{60}F_{48}$ indeed acts as a p-dopant. The EPR (**Figure 2e)** shows a distinct increase in EPR signal, indicating $C_{60}F_{48}$ increases the number of unpaired electrons in p(g3T2). UPS data in **Figure 2f** shows $C_{60}F_{48}$ is a more effective p-dopant than O_2, through a systematic increase in the work function from 4.0 eV, 4.3 eV, to 4.9 eV, for degassed-CF, ambient-CF, and degassed-CF:$C_{60}F_{48}$ (100 mol%), respectively. Additionally, the HOMO onset shifts towards the Fermi energy in order of degassed-CF, ambient-CF, and degassed-CF:$C_{60}F_{48}$ (100 mol%). UV-Vis-NIR absorbance (**Figure 2g**) further supports doping because the polaron/bipolaron absorbance between 1.6 eV and 0.5 eV increases in intensity in the same order (degassed-CF, ambient-CF, and degassed-CF:$C_{60}F_{48}$ (100 mol%)). A decrease in absorbance/peak intensity at ≈2.2 eV is consistent with polaron/bipolaron formation, indicating reduction in the neutral state with $C_{60}F_{48}$. EPR, UPS and UV-Vis confirm that p-doping mechanisms underpin OECT V_T shift, increase in μ, and increase in the μC* product: $C_{60}F_{48}$ p-dopes via integer charge transfer to accept electrons from the host,[76,77,78,79,80,81] donating holes that first fill deep and shallow localized trap states, and, once filled, the donated holes are free carriers in delocalized states. Therefore, V_T shifts[82] because it is the V_G required to fill the trap states, and I_{ON} increases from a higher carrier density. While technically the V_T shift can be used to calculate the density of trap states filled by the dopant, it is not a straightforward calculation in OECTs; ambiguity in V_T values in OECTs come from the non-linearity relationship the square

root of the drain current ($\sqrt{I_D}$) and V_G, which conflicts with the model used to extract V_T.[83, 84,85] Further evidence that $C_{60}F_{48}$ is an effective chemical p-dopant is the increase in I_{OFF} (**Figure S7**) at very high doping concentrations, because $C_{60}F_{48}$ increases OMIEC conductivity, and decrease in μ and the μC* product (**Figure S8**) because very high doping concentrations introduces scattering.[71, 75]

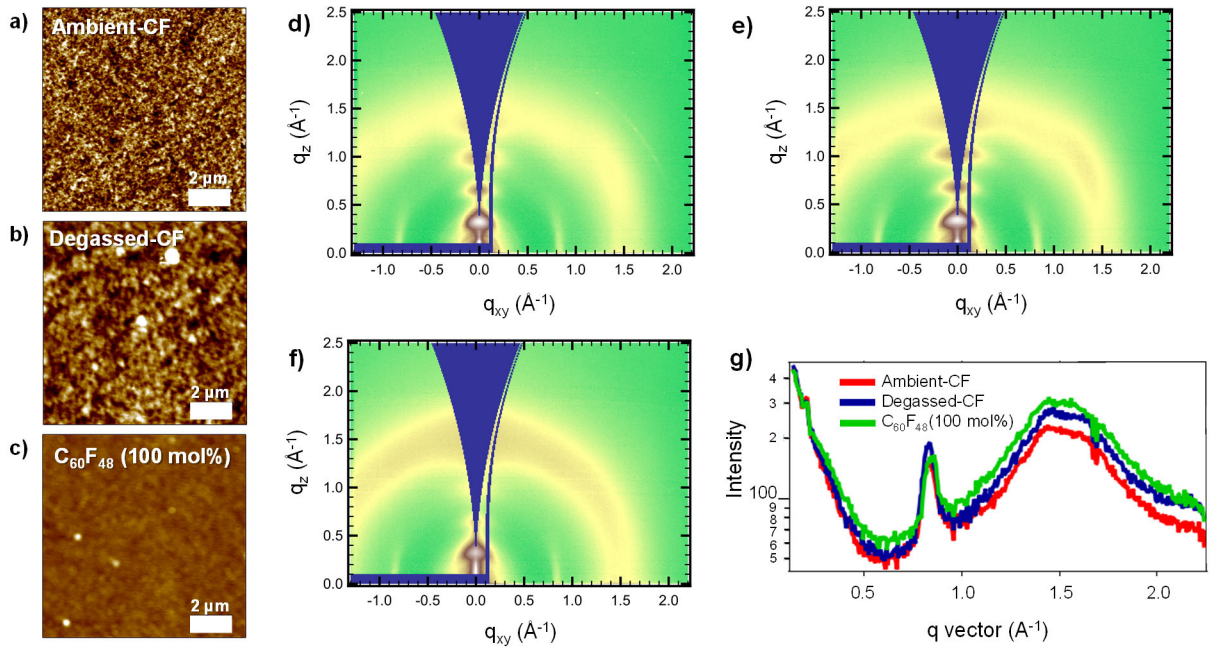

Figure 3. **Chemical p-doping influences morphology.** Atomic force microscopy images showing surface topography in the OECT channel for p(g3T2) thin-films prepared from (a) ambient-CF, (b) degassed-CF and (c) degassed-CF:$C_{60}F_{48}$(100 mol%). Grazing Incidence Wide Angle X-ray (GIWAXS) 2D detector images of p(g3T2) thin-films prepared with (d) ambient-CF, (e) degassed-CF and (f) degassed-CF:$C_{60}F_{48}$(100 mol%). The thickness of the p(g3T2) thin-films are 108 nm, 101 nm, and 33 nm for ambient-CF, degassed-CF and degassed-CF:$C_{60}F_{48}$(100 mol%), respectively. Thicknesses are average values taken from 5 values measured with a Dektak. (g) Corresponding in plane line cut of the GIWAXS data.

Improvements in μ and therefore the μC* product can occur because morphology changes occur synergistically with the p-doping shown in EPR, UPS and UV-Vis.[62, 63, 71, 86] Atomic force microscopy (AFM) and grazing-Incidence wide-angle X-ray scattering (GIWAXS) were used to elucidate differences in p(g3T2) thin-film morphology when processed from degassed-CF, ambient-CF and degassed-CF:$C_{60}F_{48}$. AFM in **Figure 3a-c** and **Table 2** show root mean squared (RMS) roughness values of 14.8 nm and 18.5 nm for ambient-CF and degassed-CF, respectively, compared to 2.2 nm for degassed-CF:$C_{60}F_{48}$. Reduction in RMS in doped organic thin-films have been observed before.[62] GIWAXS supports AFM data by showing similar morphologies for degassed-CF and ambient-CF p(g3T2) thin-films, and comparatively dramatic changes in degassed-CF:$C_{60}F_{48}$ morphology. First, **Figure 3d-e** shows p(g3T2) thin-films processed from ambient-CF and degassed-CF films are qualitatively similar, adopting a predominantly edge on orientation with out of plane lamellar stacking peaks, that corresponds with reported literature.[66] However, we find the degassed-CF lattice is tighter in real space, and the ambient-CF lattice spacing has expanded by 4 %; ambient-CF lattice shifts to lower q (**Table 3**), and quantitative analysis fitting of the (100) lamellar peak **Figure S9** reveals a 4 % expansion that suggests ambient-CF film is lightly p-doped relative to degassed-CF. Second, **Figure 3e-f** shows degassed-CF:$C_{60}F_{48}$ has stronger scattering at 1.7 A^{-1}, consistent with a dramatic increase in the π-π stacking. The significant increase in π-crystallinity may be because there are a greater number of delocalised charge carriers in p(g3T2) processed from degassed-CF:$C_{60}F_{48}$.[87] Additionally, the π-π stacking is out of plane, and the π crystals are not growing out of the existing lamellar crystals.

While EPR, UPS and UV-Vis show that $C_{60}F_{48}$ is a more effective p-dopant than O_2, and AFM and GIWAXS show $C_{60}F_{48}$ changes morphology, it is difficult to disentangle whether p-

doping or morphology change is the dominant mechanism underpinning the superior OECT performance.[62, 63] Experimental and comparative computerized Fourier transform infrared (FTIR) spectroscopy were used to elucidate contributions from synergistic morphology changes and p-doping. Computed spectra (scaled B3LYP/6-31G*) of neutral p(g3T2) show only FTIR from thin-films processed from degassed-CF agree with the neutral state (**Figure S10** and **S11**). On the other hand, computed spectra of oxidized p(g3T2) show good agreement between the new peaks measured in ambient-CF and degassed-CF:$C_{60}F_{48}$ FTIR and the oxidized state (**Figure S10**). The vibrational modes are a combination of C=C stretches in the polymer backbone, accompanied by C-H oscillations, or involvement from the truncated alkoxy chains (**Figure S11**). The new peaks in ambient-CF are well-aligned with those in degassed-CF:$C_{60}F_{48}$ (**Figure S12**), suggesting that FTIR changes are unlilely to be morphological because they are not drastically different for the large fullerene dopant, compared to a small O_2 molecule. The latter indicates p-doping mechanisms may be more dominant for OECT performance, compared to morphological changes.

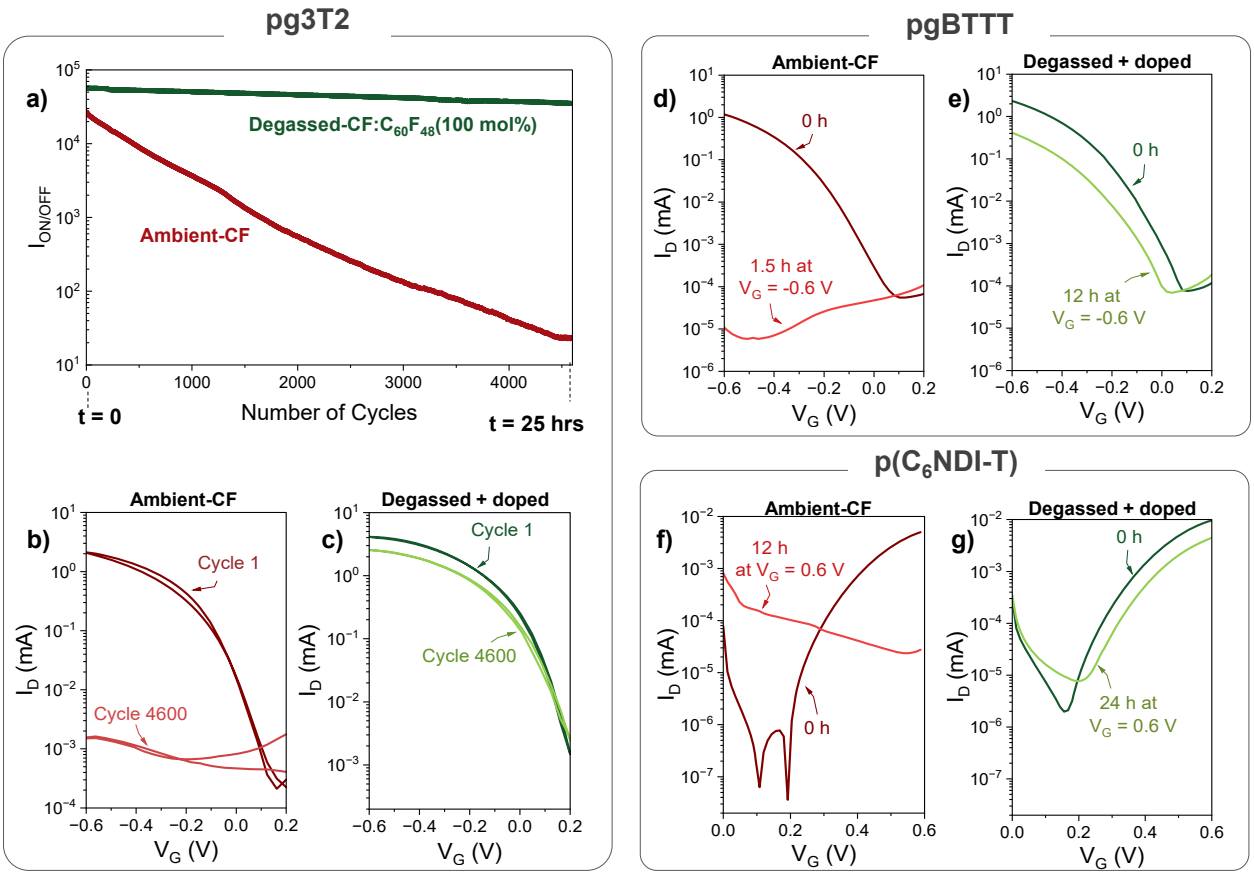

Figure 4. Solvent degassing with chemical p-doping improves organic electrochemical transistor stability. (a) 25-hour stability tests comparing on-off ratio ($I_{ON/OFF}$) degradation as a function of time, in p(g3T2) OECTs processed from ambient-CF and degassed-CF:$C_{60}F_{48}$(100 mol%). The stability test measures a transfer curves every 15 s for 25 h, with V_G swept from 0.2 V to -0.6 V, and V_D fixed at V_D = -0.6 V, for a minimum of 4600 cycles per system. The data indicates p(g3T2) OECTs processed from degassed solvent and chemically p-doped and significantly more stable than those processed from ambient-CF. (b) Comparison of the initial and final transfer curves for p(g3T2) OECTs processed from ambient-CF. (c) The initial transfer curve in the stability test, compared with the 4600th transfer curve in the stability test, for p(g3T2) OECTs processed from degassed-CF:$C_{60}F_{48}$(100 mol%). (d) and (e) show bias stress stability tests in p-type pgBTTT OECTs, where V_G = -0.6 V was applied constantly for the 12 h, with a transfer curve measured every 5 minutes. Transfer curves were measured from V_G = 0.2 V to =-0.8 V, and V_D fixed at V_D = -0.7 V. The transfer curves shown in (d) are the first transfer curve at 0 h and transfer curve after 1.5 h for pgBTTT OECTs processed from ambient-CF. The transfer curves shown in (e) are the first and last (12 h) transfer cuvres for pgBTTT OECTs processed from

degassed-CF:$C_{60}F_{48}$(300 mol%). (f) and (g) show bias stress stability tests in n-type p(C_6NDI-T) OECTs, where V_G = 0.6 V was applied constantly for the 24 h, with a transfer curve measured every 5 minutes. Transfer curves were measured from V_G = 0 V to = 0.6 V, and V_D fixed at V_D = 0.6 V. The transfer curves shown in (d) are the first transfer curve at 0 h and transfer curve at 12 h for p(C_6NDI-T) OECTs processed from ambient-CF. The transfer curves shown in (e) are the first and last (24 h) transfer curves for p(C_6NDI-T) OECTs processed from degassed-CF:TBA-OH(400 mol%).

It has not been explored yet as to whether pre-oxidizing via chemical p-doping, or "pre-doping", protects OMIECs against further oxidation with O_2 in air and water that causes OECT instability.[29, 40,35, 41, 42,42,39] Additionally, it is essential that the solvent degassing plus chemical p-doping technique works in air and water,[32, 33, 34] and O_2 has been removed from this study up to this point. To address these points, we first tested the p(g3T2) OECTs outside the glovebox in water-based electrolyte, 0.1 mol/L $NaCl_{aq.}$, and next in stability tests in air and water. **Figure S13, Figure S14** and **Table 1** shows that p(g3T2) OECTs processed from degassed-CF, ambient-CF, and degassed-CF:$C_{60}F_{48}$(100 mol%) and measured in air and water follow the same performance improvements as OECTs in an inert environment. Namely, degassed-CF:$C_{60}F_{48}$ results in the most remarkable improvements, with the $m_{gm}C^*$ product increasing from 203 F/cmVs to 281 F/cmVs and 1160 F/cmVs for p(g3T2) processed from degassed-CF, ambient-CF and degassed-CF:$C_{60}F_{48}$(100 mol%), respectively. g_m increases in order of degassed-CF, to ambient-CF, to degassed-CF:$C_{60}F_{48}$(100 mol%), and $I_{ON/OFF}$ improves, up to a maximum of 1.38 ´10^5 with the $C_{60}F_{48}$. **Table 3** compares p(g3T2) results to other p-type OECTs systems in the literature. Next, **Figure 4a-c** and **Figure S15** show the remarkable impact the two-step technique has on OECT stability. Ambient-CF $I_{ON/OFF}$ ratio decreases from 2.75´10^4 A to less than an order of magnitude

after 25 h, and **Figure S15a** shows I_{ON} reduces within the first few h of testing, decreasing from 2.1 mA to $1.8´10^{-3}$ mA after 10 h of cycling transfer curves with V_D = -0.6 V and V_G from 0.2 V to -0.6 V. In contrast, I_{ON} only reduces from 4.14 mA to 2.60 mA after 25 h of cycling for the degassed-CF:$C_{60}F_{48}$(100 mol%) OECTs (**Figure S15b**), and $I_{ON/OFF}$ ratio remains in the same order of magnitude (from $5.6´10^4$ to $3.4´10^4$) after 25 h. Importantly, V_T is significantly more stable in the $C_{60}F_{48}$ p-doped devices, shifting by only 0.01 V after 25 h (**Figure S15d-e**). The significant improvement in OECT stability for degassed-CF:$C_{60}F_{48}$(100 mol%) may be explained by pre-oxidized polymers being less susceptible to oxidation in air and water, because energetics such as IE and work function have changed, and the oxidized conditions change the chemical equilibrium via Le Chatelier's principle. While how susceptible OECTs are to O_2 oxidation also depends on voltage, 'pre-doping' from O_2 is unlikely to have this effect because it can be unstable. Specifically, O_2 doping stability depends on the host system, the location of the O_2 (crystallites or amorphous), packing density, dynamic structure and the kinetics of the O_2 moving in and out of the organic layer. Unstable O_2 during stability testing may increase O_2 concentration, resulting in further ORR and compounds that form trap states during bias stressing. The pre-doping hypothesis is further supported by the fact it is not possible to chemically p-dope p(g3T2) to achieve these remarkable results, without first removing O_2 (i.e., oxidation) via degassing. Finally, although n-doped OECTs have been successfully demonstrated in air and water,[88] the data here is the first to report successful chemical p-doping in OECTs and OMIECs operating in air and water.[28, 89]

The generality of the combined chemical doping and solvent-degassing technique was verified by testing other material systems. First, a different solvent, 1,2-dichlorobenzene (DCB), was used with p(g3T2). **Figure S16** shows p(g3T2) OECTs made with ambient-DCB, degassed-

DCB, and degassed-DCB:$C_{60}F_{48}$(100 mol%), tested in inert conditions (i.e., with [BMIM][BF_4] inside a nitrogen glovebox). Ambient-DCB OECTs have high I_{OFF}, demonstrating they are p-doped, while degassed-DCB reduces I_{OFF} and shifts V_T, showing that degassed-DCB OECTs are less doped when O_2 is removed from the solvent. $C_{60}F_{48}$ further enhances the transistor still: a sharper subthreshold slope (SS) and turn on, indicating a more pronounced g_m. Second, a different polymer, glycolated polythiophene p(g2T2-g4T2) (**Figure 4d**),[66] was processed from degassed-CF and degassed-CF:$C_{60}F_{48}$ and tested in inert conditions. **Figure S17** shows the results, indicating the same trends as p(g3T2) in **Figure 2b-d**: degassing CF and p-doping with $C_{60}F_{48}$ in the most extreme case results in a three order of magnitude increase in I_{ON}, a corresponding g_m increases from 0.02 to 16.4 mS, and improved $I_{ON/OFF}$ ratio. Third, we tested another polymer, pgBTTT (**Figure S18a**)[90], and another p-dopant tris(pentafluorophenyl)borane ($B(C_6F_5)_3$) (**Figure S18b**), in air and water with a 0.1 mol/L $NaCl_{aq.}$ electrolyte. **Figure S18d-h** show that, in both cases, g_m increases in pgBTTT OECTs processed from degassed-CF and p-doped with either $C_{60}F_{48}$ or $B(C_6F_5)_3$, when compared to OECTs processed from ambient-CF, and V_T shifts towards 0 V, consistent with successful p-doping. I_{OFF} also increases in pgBTTT OECTs processed from degassed-CF:$C_{60}F_{48}$(100 mol%) OECTs. Next, **Figure 4 d-e** show the impact on pgBTTT stability in air and water, where pgBTTT OECTs processed from ambient-CF and degassed-CF:$C_{60}F_{48}$(100 mol%) are subjected to much harsher biasing conditions, compared to the typical cycling OECT tests, like those shown for pg3T2 in **Figure 4a-c**. Namely, V_G = -0.6 V is applied constantly for 12 h, with a transfer curve measured quickly every 5 minutes to monitor the impact from biasing. **Figure 4d-e** and **Figure S19a** show that ambient-CF OECTs are not functional after 1.5 h. Comparatively, pgBTTT OECTs processed from degasses-CF:$C_{60}F_{48}$(100 mol%) are still functional after 12 h. Finally, we tested the impact of degassing and doping on stability in n-type

OECTs: p(C_6NDI-T)[91] n-doped with TBA-OH.[88] Here, V_G = 0.6 V was applied for 24 h. **Figure 4f-g** and **Figure S19b** show that, while ambient-CF OECTs are not functional, p(C_6NDI-T) OECTs processed from degassed-CF:TBA-OH(100 mol%) are fully operational after 24 h of a high, constant gate bias, with I_{ON} only decreasing from 9.6 μA to 4.4 μA. To the best of our knowledge, the stability tests reported in this manuscript are the most rigorous OECT stability tests reported to-date, and all the polymers processed here using the solvent degassing and chemical doping technique realize the most stable OECTs reported to-date in air and water.[92, 93] Importantly, all aforedescribed systems that support the generality of this technique are not optimized, and every dopant/polymer/solvent combination requires careful optimization because dopant effectiveness depends on solvent, solvents impact thin-film morphology, and dopant concentration should not introduce structural disorder and scattering that reduces μ. Each of these systems therefore has significant potential for further work, while demonstrating the effectiveness of solvent degassing and chemical doping with different polymers, solvent, dopant and operating environments (i.e., inert vs. ambient/water).

In conclusion, we show using ultraviolet photoelectron spectroscopy, density functional theory, and electron paramagnetic resonance that oxygen dissolved in chloroform acts as a p-dopant in OECTs and OMIECs. While oxygen p-doping impacts OECT electronic performance, the presence of oxygen also jeopardizes OECT stability. We approach this problem by introducing a new, two-step strategy, that simultaneously removes the risks from oxygen, while enhancing OECT stability and operating metrics. First, the solvent is degassed using a freeze-pump-thaw method. Second, the OMIEC is doped. Improvements in the μC* product, g_m, μ and $I_{ON/OFF}$ are shown to arise from synergistic p-doping and morphology changes, using ultraviolet photoelectron

spectra, electron paramagnetic resonance, ultraviolet-visible atomic force microscopy, grazing-incidence wide-angle X-ray scattering and Fourier transform infrared spectroscopy. This strategy can also be used to tune V_T, works in air and water environments, in more than one solvent, with more than one polymer, and more than one dopant. A key finding is that degassing combined with chemical doping showcases the most stable p-type and n-type OECTs operating in air and water to-date. The improvement in OECT stability may be explained by 'pre-doping', that makes p-type OMIECs more difficult to oxidize, and n-type OMIECs harder to reduce and therefore less reactive in oxygen and water. A crucial part of improving OECT stability using chemical doping is to first degases the solvent. Overall, the data presented here suggests this simple, low-cost and easily implemented strategy could be a broadly applicable tool for improving key figures of merit in accumulation mode OMIECs, and overcome OMIECs and OECTs stability challenges.

References

1. Fan J, Forero Pico AA, Gupta M. A functionalization study of aerosol jet printed organic electrochemical transistors (OECTs) for glucose detection. *Materials Advances* 2021, **2**(22)**:** 7445-7455.

2. Guo K, Wustoni S, Koklu A, Díaz-Galicia E, Moser M, Hama A*, et al.* Rapid single-molecule detection of COVID-19 and MERS antigens via nanobody-functionalized organic electrochemical transistors. *Nature Biomedical Engineering* 2021, **5**(7)**:** 666-677.

3. Lee H, Lee S, Lee W, Yokota T, Fukuda K, Someya T. Ultrathin Organic Electrochemical Transistor with Nonvolatile and Thin Gel Electrolyte for Long-Term Electrophysiological Monitoring. *Advanced Functional Materials* 2019, **29**(48)**:** 1906982.

4. Rivnay J, Inal S, Salleo A, Owens RM, Berggren M, Malliaras GG. Organic electrochemical transistors. *Nature Reviews Materials* 2018, **3:** 17086.

5. Tyrrell JE, Boutelle MG, Campbell AJ. Measurement of Electrophysiological Signals In Vitro Using High-Performance Organic Electrochemical Transistors. *Advanced Functional Materials* 2021, **31**(1)**:** 2007086.

6. Khodagholy D, Doublet T, Quilichini P, Gurfinkel M, Leleux P, Ghestem A*, et al.* In vivo recordings of brain activity using organic transistors. *Nature Communications* 2013, **4:** 1575.

7. Wang H, Zhao Q, Ni Z, Li Q, Liu H, Yang Y*, et al.* A Ferroelectric/Electrochemical Modulated Organic Synapse for Ultraflexible, Artificial Visual-Perception System. *Advanced Materials* 2018, **30**(46)**:** 1803961.

8. Torricelli F, Adrahtas DZ, Bao Z, Berggren M, Biscarini F, Bonfiglio A*, et al.* Electrolyte-gated transistors for enhanced performance bioelectronics. *Nature Reviews Methods Primers* 2021, **1**(1)**:** 66.

9. Gumyusenge A. Organic Iono-Electronics, a New Front for Semiconducting Polymers to Shine. *Accounts of Materials Research* 2022, **3**(7)**:** 669-671.

10. Juzekaeva E, Nasretdinov A, Battistoni S, Berzina T, Iannotta S, Khazipov R*, et al.* Coupling Cortical Neurons through Electronic Memristive Synapse. *Advanced Materials Technologies* 2019, **4**(1)**:** 1800350.

11. Fuller EJ, Keene ST, Melianas A, Wang Z, Agarwal S, Li Y*, et al.* Parallel programming of an ionic floating-gate memory array for scalable neuromorphic computing. *Science* 2019, **364**(6440)**:** 570-574.

12. Gerasimov JY, Gabrielsson R, Forchheimer R, Stavrinidou E, Simon DT, Berggren M*, et al.* An Evolvable Organic Electrochemical Transistor for Neuromorphic Applications. *Advanced Science* 2019, **6**(7)**:** 1801339.

13. Gkoupidenis P, Koutsouras DA, Malliaras GG. Neuromorphic device architectures with global connectivity through electrolyte gating. *Nature Communications* 2017, **8:** 15448.

14. Gkoupidenis P, Schaefer N, Garlan B, Malliaras GG. Neuromorphic Functions in PEDOT:PSS Organic Electrochemical Transistors. *Advanced Materials* 2015, **27**(44)**:** 7176-7180.

15. van de Burgt Y, Lubberman E, Fuller EJ, Keene ST, Faria GC, Agarwal S*, et al.* A non-volatile organic electrochemical device as a low-voltage artificial synapse for neuromorphic computing. *Nature Materials* 2017, **16**(4)**:** 414-418.

16. Ghittorelli M, Lingstedt L, Romele P, Crăciun NI, Kovács-Vajna ZM, Blom PWM*, et al.* High-sensitivity ion detection at low voltages with current-driven organic electrochemical transistors. *Nature Communications* 2018, **9**(1)**:** 1441.

17. Lee Y, Lee T-W. Organic Synapses for Neuromorphic Electronics: From Brain-Inspired Computing to Sensorimotor Nervetronics. *Accounts of Chemical Research* 2019, **52**(4)**:** 964-974.

18. Marks A, Griggs S, Gasparini N, Moser M. Organic Electrochemical Transistors: An Emerging Technology for Biosensing. *Advanced Materials Interfaces* 2022, **9**(6)**:** 2102039.

19. Dufil G, Bernacka-Wojcik I, Armada-Moreira A, Stavrinidou E. Plant Bioelectronics and Biohybrids: The Growing Contribution of Organic Electronic and Carbon-Based Materials. *Chemical Reviews* 2022, **122**(4)**:** 4847-4883.

20. Strand EJ, Bihar E, Gleason SM, Han S, Schreiber SW, Renny MN*, et al.* Printed Organic Electrochemical Transistors for Detecting Nutrients in Whole Plant Sap. *Advanced Electronic Materials* 2022, **8**(4)**:** 2100853.

21. Skowrons M, Schander A, Negron AGP, Lüssem B. The Trade-Off between Transconductance and Speed for Vertical Organic Electrochemical Transistors. *Advanced Electronic Materials* 2024**:** 2300673.

22. Uguz I, Ohayon D, Yilmaz S, Griggs S, Sheelamanthula R, Fabbri JD*, et al.* Complementary integration of organic electrochemical transistors for front-end amplifier circuits of flexible neural implants. *Science Advances* 2024, **10**(12)**:** eadi9710.

23. Shiri P, Dacanay EJS, Hagen B, Kaake LG. Vogel–Tammann–Fulcher model for charging dynamics in an organic electrochemical transistor. *Journal of Materials Chemistry C* 2019, **7**(41)**:** 12935-12941.

24. Wang S, Chen X, Zhao C, Kong Y, Lin B, Wu Y*, et al.* An organic electrochemical transistor for multi-modal sensing, memory and processing. *Nature Electronics* 2023, **6**(4)**:** 281-291.

25. Huang W, Chen J, Yao Y, Zheng D, Ji X, Feng L-W*, et al.* Vertical organic electrochemical transistors for complementary circuits. *Nature* 2023, **613**(7944)**:** 496-502.

26. Tropp J, Meli D, Rivnay J. Organic mixed conductors for electrochemical transistors. *Matter* 2023, **6:** 3132-3164.

27. Paterson AF, Anthopoulos TD. Enabling thin-film transistor technologies and the device metrics that matter. *Nat Commun* 2018, **9**(1)**:** 5264.

28. Paterson AF, Savva A, Wustoni S, Tsetseris L, Paulsen BD, Faber H*, et al.* Water stable molecular n-doping produces organic electrochemical transistors with high transconductance and record stability. *Nature communications* 2020, **11**(1)**:** 3004.

29. Xie M, Liu H, Wu M, Chen C, Wen J, Bai L*, et al.* Cycling stability of organic electrochemical transistors. *Organic Electronics* 2023**:** 106777.

30. Bidinger SL, Han S, Malliaras GG, Hasan T. Highly stable PEDOT: PSS electrochemical transistors. *Applied Physics Letters* 2022, **120**(7)**:** 073302.

31. Hidalgo Castillo TC, Moser M, Cendra C, Nayak PD, Salleo A, McCulloch I*, et al.* Simultaneous Performance and Stability Improvement of a p-Type Organic Electrochemical Transistor through Additives. *Chemistry of Materials* 2022, **34**(15)**:** 6723-6733.

32. Tropp J, Rivnay J. Design of biodegradable and biocompatible conjugated polymers for bioelectronics. *Journal of Materials Chemistry C* 2021, **9**(39)**:** 13543-13556.

33. Nawaz A, Liu Q, Leong WL, Fairfull-Smith KE, Sonar P. Organic Electrochemical Transistors for In Vivo Bioelectronics. *Adv Mater* 2021, **33**(49)**:** e2101874.

34. Rivnay J, Ramuz M, Leleux P, Hama A, Huerta M, Owens RM. Organic electrochemical transistors for cell-based impedance sensing. *Applied Physics Letters* 2015, **106**(4).

35. Giovannitti A, Thorley KJ, Nielsen CB, Li J, Donahue MJ, Malliaras GG*, et al.* Redox-Stability of Alkoxy-BDT Copolymers and their Use for Organic Bioelectronic Devices. *Advanced Functional Materials* 2018, **28**(17).

36. Tan STM, Giovannitti A, Melianas A, Moser M, Cotts BL, Singh D*, et al.* High-Gain Chemically Gated Organic Electrochemical Transistor. *Advanced Functional Materials* 2021, **31**(19).

37. Schafer EA, Wu R, Meli D, Tropp J, Moser M, McCulloch I*, et al.* Sources and Mechanism of Degradation in p-Type Thiophene-Based Organic Electrochemical Transistors. *ACS Applied Electronic Materials* 2022, **4**(4)**:** 1391-1404.

38. Bukas VJ, Kim HW, Sengpiel R, Knudsen K, Voss J, McCloskey BD*, et al.* Combining Experiment and Theory To Unravel the Mechanism of Two-Electron Oxygen Reduction at a Selective and Active Co-catalyst. *ACS Catalysis* 2018, **8**(12)**:** 11940-11951.

39. Zhang S, Ding P, Ruoko TP, Wu R, Stoeckel MA, Massetti M*, et al.* Toward Stable p-Type Thiophene-Based Organic Electrochemical Transistors. *Advanced Functional Materials* 2023.

40. Zhang S, Ding P, Ruoko TP, Wu R, Stoeckel MA, Massetti M*, et al.* Toward Stable p-Type Thiophene-Based Organic Electrochemical Transistors. *Advanced Functional Materials* 2023, **33:** 2302249.

41. Decataldo F, Gualandi I, Tessarolo M, Scavetta E, Fraboni B. Transient-doped organic electrochemical transistors working in current-enhancing mode as sensing devices for low concentration of oxygen dissolved in solution. *APL Materials* 2020, **8**(9).

42. Giovannitti A, Rashid RB, Thiburce Q, Paulsen BD, Cendra C, Thorley K*, et al.* Energetic Control of Redox-Active Polymers toward Safe Organic Bioelectronic Materials. *Adv Mater* 2020, **32**(16)**:** e1908047.

43. Apel K, Hirt H. Reactive oxygen species: metabolism, oxidative stress, and signal transduction. *Annu Rev Plant Biol* 2004, **55:** 373-399.

44. Dimov IB, Moser M, Malliaras GG, McCulloch I. Semiconducting Polymers for Neural Applications. *Chemical Reviews* 2022, **122**(4)**:** 4356-4396.

45. Watt BE, Proudfoot AT, Vale JA. Hydrogen peroxide poisoning. *Toxicological reviews* 2004, **23:** 51-57.

46. Hüppi P. The role of oxygen in health and disease–a series of reviews. *Pediatr Res* 2009, **65**(3)**:** 261-268.

47. Apel K, Hirt H. Reactive oxygen species: metabolism, oxidative stress, and signal transduction. *Annu Rev Plant Biol* 2004, **55:** 373-399.

48. Scaccabarozzi AD, Basu A, Aniés F, Liu J, Zapata-Arteaga O, Warren R*, et al.* Doping Approaches for Organic Semiconductors. *Chem Rev* 2022, **122**(4)**:** 4420-4492.

49. Lu C-K, Meng H-F. Hole doping by molecular oxygen in organic semiconductors: Band-structure calculations. *Physical Review B* 2007, **75**(23).

50. Liao H-H, Yang C-M, Liu C-C, Horng S-F, Meng H-F, Shy J-T. Dynamics and reversibility of oxygen doping and de-doping for conjugated polymer. *Journal of Applied Physics* 2008, **103**(10).

51. Sperlich A, Kraus H, Deibel C, Blok H, Schmidt J, Dyakonov V. Reversible and Irreversible Interactions of Poly(3-hexylthiophene) with Oxygen Studied by Spin-Sensitive Methods. *The Journal of Physical Chemistry B* 2011, **115**(46)**:** 13513-13518.

52. Schafferhans J, Baumann A, Wagenpfahl A, Deibel C, Dyakonov V. Oxygen doping of P3HT:PCBM blends: Influence on trap states, charge carrier mobility and solar cell performance. *Org Electron* 2010, **11**(10)**:** 1693-1700.

53. Moser M, Ponder Jr. JF, Wadsworth A, Giovannitti A, McCulloch I. Materials in Organic Electrochemical Transistors for Bioelectronic Applications: Past, Present, and Future. *Advanced Functional Materials* 2018, **0**(0)**:** 1807033.

54. Tropp J, Meli D, Rivnay J. Organic mixed conductors for electrochemical transistors. *Matter* 2023.

55. Meijer EJ, Detcheverry C, Baesjou PJ, van Veenendaal E, de Leeuw DM, Klapwijk TM. Dopant density determination in disordered organic field-effect transistors. *Journal of Applied Physics* 2003, **93**(8)**:** 4831-4835.

56. Barf MM, Benneckendorf FS, Reiser P, Bäuerle R, Köntges W, Müller L*, et al.* Compensation of Oxygen Doping in p-Type Organic Field-Effect Transistors Utilizing Immobilized n-Dopants. *Advanced Materials Technologies* 2020, **6**(2).

57. Zhu G, Chen J, Duan J, Liao H, Zhu X, Li Z*, et al.* Fluorinated alcohol-processed N-type organic electrochemical transistor with high performance and enhanced stability. *ACS Applied Materials & Interfaces* 2022, **14**(38)**:** 43586-43596.

58. Duan C, Cai W, Hsu BB, Zhong C, Zhang K, Liu C*, et al.* Toward green solvent processable photovoltaic materials for polymer solar cells: the role of highly polar pendant groups in charge carrier transport and photovoltaic behavior. *Energy & Environmental Science* 2013, **6**(10)**:** 3022-3034.

59. Duong DT, Tuchman Y, Chakthranont P, Cavassin P, Colucci R, Jaramillo TF*, et al.* A Universal Platform for Fabricating Organic Electrochemical Devices. *Advanced Electronic Materials* 2018, **4**(7).

60. Savva A, Ohayon D, Surgailis J, Paterson AF, Hidalgo TC, Chen X*, et al.* Solvent Engineering for High-Performance n-Type Organic Electrochemical Transistors. *Advanced Electronic Materials* 2019, **5**(8).

61. Niazi MR, Li R, Qiang Li E, Kirmani AR, Abdelsamie M, Wang Q*, et al.* Solution-printed organic semiconductor blends exhibiting transport properties on par with single crystals. *Nature communications* 2015, **6**(1)**:** 8598.

62. Panidi J, Paterson AF, Khim D, Fei Z, Han Y, Tsetseris L*, et al.* Remarkable enhancement of the hole mobility in several organic small-molecules, polymers, and small-molecule: polymer blend transistors by simple admixing of the Lewis acid P-dopant B (C6F5) 3. *Advanced Science* 2018, **5**(1)**:** 1700290.

63. Paterson AF, Treat ND, Zhang W, Fei Z, Wyatt-Moon G, Faber H*, et al.* Small molecule/polymer blend organic transistors with hole mobility exceeding 13 cm2 V− 1 s− 1. *Advanced Materials* 2016, **28**(35)**:** 7791-7798.

64. Moia D, Giovannitti A, Szumska AA, Maria IP, Rezasoltani E, Sachs M*, et al.* Design and evaluation of conjugated polymers with polar side chains as electrode materials for electrochemical energy storage in aqueous electrolytes. *Energy & Environmental Science* 2019, **12**(4)**:** 1349-1357.

65. Gladisch J, Stavrinidou E, Ghosh S, Giovannitti A, Moser M, Zozoulenko I*, et al.* Reversible Electronic Solid–Gel Switching of a Conjugated Polymer. *Advanced Science* 2020, **7**(2)**:** 1901144.

66. Moser M, Hidalgo TC, Surgailis J, Gladisch J, Ghosh S, Sheelamanthula R*, et al.* Side Chain Redistribution as a Strategy to Boost Organic Electrochemical Transistor Performance and Stability. *Advanced Materials* 2020, **32**(37)**:** 2002748.

67. Liang Z, Boland MJ, Butrouna K, Strachan DR, Graham KR. Increased power factors of organic–inorganic nanocomposite thermoelectric materials and the role of energy filtering. *Journal of materials chemistry A* 2017, **5**(30)**:** 15891-15900.

68. Thorley KJ, Le H, Song Y, Anthony JE. Unravelling the major factors in photo-oxidative stability of anthradithiophene derivatives. *J Mater Chem C* 2022, **10**(42)**:** 15861-15871.

69. Bard AJ, Faulkner LR, White HS. *Electrochemical methods: fundamentals and applications*. John Wiley & Sons, 2022.

70. Wijeyasinghe N, Eisner F, Tsetseris L, Lin Y-H, Seitkhan A, Li J*, et al.* p-Doping of Copper(I) Thiocyanate (CuSCN) Hole-Transport Layers for High-Performance Transistors and Organic Solar Cells. *Advanced Functional Materials* 2018, **28**(31).

71. Paterson AF, Lin YH, Mottram AD, Fei Z, Niazi MR, Kirmani AR*, et al.* The Impact of Molecular p-Doping on Charge Transport in High-Mobility Small-Molecule/Polymer Blend Organic Transistors. *Advanced Electronic Materials* 2018, **4**(10)**:** 1700464.

72. Scaccabarozzi AD, Scuratti F, Barker AJ, Basu A, Paterson AF, Fei Z*, et al.* Understanding Charge Transport in High-Mobility p-Doped Multicomponent Blend Organic Transistors. *Advanced Electronic Materials* 2020, **6**(10)**:** 2000539.

73. Kim HW, Bukas VJ, Park H, Park S, Diederichsen KM, Lim J*, et al.* Mechanisms of Two-Electron and Four-Electron Electrochemical Oxygen Reduction Reactions at Nitrogen-Doped Reduced Graphene Oxide. *ACS Catalysis* 2019, **10**(1)**:** 852-863.

74. Nielsen CB, Giovannitti A, Sbircea D-T, Bandiello E, Niazi MR, Hanifi DA*, et al.* Molecular Design of Semiconducting Polymers for High-Performance Organic Electrochemical Transistors. *Journal of the American Chemical Society* 2016, **138**(32)**:** 10252-10259.

75. Lussem B, Keum C-M, Kasemann D, Naab B, Bao Z, Leo K. Doped organic transistors. *Chemical reviews* 2016, **116**(22)**:** 13714-13751.

76. Smets Y, Stark CB, Schmitt F, Edmonds MT, Lach S, Wright CA*, et al.* Doping efficiency and energy-level scheme in C60F48-doped zinc-tetraphenylporphyrin films. *Org Electron* 2013, **14**(1)**:** 169-174.

77. Edmonds MT, Wanke M, Tadich A, Vulling HM, Rietwyk KJ, Sharp PL*, et al.* Surface transfer doping of hydrogen-terminated diamond by C60F48: Energy level scheme and doping efficiency. *J Chem Phys* 2012, **136**(12)**:** 124701.

78. Tada T, Uchida N, Kanayama T, Hiura H, Kimoto K. Charge-transfer doping by fullerenes on oxidized Si surfaces. *J Appl Phys* 2007, **102**(7).

79. Tadich A, Edmonds MT, Ley L, Fromm F, Smets Y, Mazej Z*, et al.* Tuning the charge carriers in epitaxial graphene on SiC(0001) from electron to hole via molecular doping with C60F48. *Appl Phys Lett* 2013, **102**(24)**:** 241601.

80. Rietwyk KJ, Wanke M, Vulling HM, Edmonds MT, Sharp PL, Smets Y*, et al.* Fluorination of the diamond surface by photoinduced dissociation of C60F48. *Physical Review B* 2011, **84**(3)**:** 035404.

81. Paterson AF, Lin Y-H, Mottram AD, Fei Z, Niazi MR, Kirmani AR*, et al.* The Impact of Molecular p-Doping on Charge Transport in High-Mobility Small-Molecule/Polymer Blend Organic Transistors. *Adv Electron Mater* 2017, **4**(10)**:** 1700464.

82. Jurchescu OD. Precision doping to heal traps. *Nature Materials* 2021, **20**(11)**:** 1458-1460.

83. Skowrons M, Dahal D, Paudel PR, Lüssem B. Depletion Type Organic Electrochemical Transistors and the Gradual Channel Approximation. *Advanced Functional Materials*, **n/a**(n/a)**:** 2303324.

84. Marková A, Střítеský S, Weiter M, Vala M. Serial Resistance Effect on Organic Electrochemical Transistors' Transconductance. *IEEE Sensors Journal* 2023**:** 1-1.

85. Shahi M, Le VN, Alarcon Espejo P, Alsufyani M, Kousseff CJ, McCulloch I*, et al.* The organic electrochemical transistor conundrum when reporting a mixed ionic–electronic transport figure of merit. *Nature Materials* 2023.

86. Paterson AF, Tsetseris L, Li R, Basu A, Faber H, Emwas AH*, et al.* Addition of the Lewis acid Zn (C6F5) 2 enables organic transistors with a maximum hole mobility in excess of 20 cm2 V− 1 s− 1. *Advanced Materials* 2019, **31**(27)**:** 1900871.

87. Quill TJ, LeCroy G, Marks A, Hesse SA, Thiburce Q, McCulloch I*, et al.* Charge Carrier Induced Structural Ordering And Disordering in Organic Mixed Ionic Electronic Conductors. *Advanced Materials*, **n/a**(n/a)**:** 2310157.

88. Le VN, Bombile JH, Rupasinghe GS, Baustert KN, Li R, Maria IP*, et al.* New Chemical Dopant and Counterion Mechanism for Organic Electrochemical Transistors and Organic Mixed Ionic–Electronic Conductors. *Advanced Science* 2023, **10:** 2207694.

89. Le VN, Bombile JH, Rupasinghe GS, Baustert KN, Li R, Maria IP*, et al.* New Chemical Dopant and Counterion Mechanism for Organic Electrochemical Transistors and Organic Mixed Ionic–Electronic Conductors. *Advanced Science* 2023**:** 2207694.

90. Hallani RK, Paulsen BD, Petty AJ, II, Sheelamanthula R, Moser M, Thorley KJ*, et al.* Regiochemistry-Driven Organic Electrochemical Transistor Performance Enhancement in Ethylene Glycol-Functionalized Polythiophenes. *Journal of the American Chemical Society* 2021, **143**(29)**:** 11007-11018.

91. Koklu A, Wustoni S, Musteata V-E, Ohayon D, Moser M, McCulloch I*, et al.* Microfluidic integrated organic electrochemical transistor with a nanoporous membrane for amyloid-β detection. *ACS nano* 2021, **15**(5)**:** 8130-8141.

92. Zeglio E, Eriksson J, Gabrielsson R, Solin N, Inganäs O. Highly Stable Conjugated Polyelectrolytes for Water-Based Hybrid Mode Electrochemical Transistors. *Advanced Materials* 2017, **29**(19)**:** 1605787.

93. Zhang S, Ding P, Ruoko T-P, Wu R, Stoeckel M-A, Massetti M*, et al.* Toward Stable p-Type Thiophene-Based Organic Electrochemical Transistors. *Advanced Functional Materials*, **n/a**(n/a)**:** 2302249.

94. Frisch MJ, Trucks GW, Schlegel HB, Scuseria GE, Robb MA, Cheeseman JR*, et al.* Gaussian 16 Rev. C.01. Wallingford, CT; 2016.

95. Paterson AF, Li R, Markina A, Tsetseris L, MacPhee S, Faber H*, et al.* N-doping improves charge transport and morphology in the organic non-fullerene acceptor O-IDTBR. *Journal of Materials Chemistry C* 2021, **9**(13)**:** 4486-4495.

96. O'boyle NM, Tenderholt AL, Langner KM. cclib: A library for package-independent computational chemistry algorithms. *J Comput Chem* 2008, **29**(5)**:** 839-845.

97. Bernards DA, Malliaras GG. Steady-State and Transient Behavior of Organic Electrochemical Transistors. *Advanced Functional Materials* 2007, **17**(17)**:** 3538-3544.

98. Ohayon D, Druet V, Inal S. A guide for the characterization of organic electrochemical transistors and channel materials. *Chemical Society Reviews* 2023, **52**(3)**:** 1001-1023.

99. Inal S, Malliaras GG, Rivnay J. Benchmarking organic mixed conductors for transistors. *Nature communications* 2017, **8**(1)**:** 1767.

100. Khodagholy D, Rivnay J, Sessolo M, Gurfinkel M, Leleux P, Jimison LH*, et al.* High transconductance organic electrochemical transistors. *Nature Communications* 2013, **4**(1)**:** 2133.

101. Kim S-M, Kim C-H, Kim Y, Kim N, Lee W-J, Lee E-H*, et al.* Influence of PEDOT:PSS crystallinity and composition on electrochemical transistor performance and long-term stability. *Nature Communications* 2018, **9**(1)**:** 3858.

102. Liang Y, Brings F, Maybeck V, Ingebrandt S, Wolfrum B, Pich A*, et al.* Tuning Channel Architecture of Interdigitated Organic Electrochemical Transistors for Recording the Action Potentials of Electrogenic Cells. *Advanced Functional Materials* 2019, **29**(29)**:** 1902085.

103. Yan Y, Chen Q, Wu X, Wang X, Li E, Ke Y*, et al.* High-Performance Organic Electrochemical Transistors with Nanoscale Channel Length and Their Application to Artificial Synapse. *ACS Applied Materials & Interfaces* 2020, **12**(44)**:** 49915-49925.

Acknowledgements

V. N. L and A.F.P thank the National Science Foundation (NSF) through cooperative agreement number 1849213 for financial support. Department and the Center for Computational Sciences (CCS). K.N.B., M.B., J.H.B., C.R., and K.G. gratefully acknowledge support from the National Science Foundation through award number DMR-1905734. This research used beamline 11-BM (CMS) of the National Synchrotron Light Source II, a US Department of Energy (DOE) Office of Science User Facility operated for the DOE Office of Science by Brookhaven National Laboratory under contract No. DE-SC0012704. Computing resources on the Lipscomb High Performance Computing Cluster were provided by the University of Kentucky Center for Computational Sciences and Information Technology Services Research Computing.

Competing financial interests

The authors declare no competing financial interests.

Experimental Section

Density Functional Theory Calculations. Density functional theory (DFT) calculations were performed for p(g3T2)-based oligomers of 3.5 repeat units each (14 thiophene units) and six small molecules that may be found in chloroform (chlorine gas, hydrochloric acid, hydrogen peroxide, oxygen gas, phosgene, and trichloroacetic acid). The long-range corrected hybrid functional LC-ωHPBE, optimally tuned with respect to both the highest occupied molecular orbital (HOMO) and lowest unoccupied molecular orbital (LUMO) of the p(g3T2) oligomer, and the 6-31G(d) basis set were used. The geometry of the neutral and charged states (+1,-1) for each species were optimized, and an implicit solvation model utilizing the polarizable continuum model (PCM) was used to account for the chloroform solvent environment. The ionization energy (IE) and the electron affinity (EA) were calculated as the energy difference between the charged state and the neutral state. To assess accuracy of the results, calculations at MP2 level of theory on the DFT geometries were performed and all gas-phase results were compared to available experimental data. The DFT

approach presented the smallest total mean square error for the EA and IE. All calculations were performed using the Gaussian 16 Revision A.03 quantum chemical calculation package[94].

Organic electrochemical transistor preparation. All OECT devices were fabricated on 2 cm × 2 cm Borofloat glass slides cleaned by a three-step solvent sonication for 10 minutes for each step. First by sonicating with a 5 % volume fraction Decon-90 soap and DI water solution, then acetone, and lastly by isopropanol alcohol. The sonicated substrates were then blow dried by N_2 and then cleaned by ultraviolet ozone for 10 minutes using a Samco UV-1 bench top cleaner with 0.5 L/min O_2 gas flow. The source and drain electrodes were patterned by thermally evaporating a 5 nm metal Cr adhesion layer followed by 40 nm Au conduction layer using an Angstrom physical vapor deposition system with channel dimensions of 500 μm width and 50 μm length using a custom shadow mask purchased from Angstrom After thermal evaporation, the surface of the patterned substrates were activated by ultraviolet ozone for 15 minutes to increase wettability using the same bench top cleaner with 0.5 L/min O_2 gas flow followed by adhesion promotor application using (3-(trimethoxysilyl)propyl methacrylate) purchased from Tokyo Chemical Industry Co. in an isopropanol alcohol:DI water:(3-(trimethoxysilyl)propyl methacrylate) solution at a volume ratio of 100:100:3. The substrates were immersed in the adhesion promotor solution for 30 minutes, then rinsed with isopropanol alcohol and allowed to air dry. A 2 μm layer of Parylene C was deposited on the substrates using a SCS Labcoater 2 and dichloro-p-cyclophane Parylene dimer purchased from Specialty Coating Systems. After deposition, a 4 % volume fraction microsoap solution was spin coated onto the parylene coated substrates at 6000 rpm (1 rpm = $2\pi/60$ rad s^{-1}) to promote delamination of a second layer of parylene. The second 4 μm layer of Parylene C was applied using the same system to serve as a sacrificial patterning layer. Photolithography was used to pattern the Parylene C on the substrates by spin casting a 9um later of SPR 220-7 positive photoresist, exposing the substrates using a custom photomask and Suss MA6 contact aligner with a i-line UVA light source with 365nm wave length. M-26 developer was used to develop the photoresist by soaking for 5 minutes, rinsing with DI water and blow drying with N_2. Finally, a March reactive ion etcher (RIE) system was used to etch the photolithography patterned channel and contact features by O_2 reactive ion etching with 25 sccm of O_2 gas, 40 Pa pressure chamber pressure, and 300 Watt power. A thin film of the prepared polymer solutions were coated on to the OECT substrates by statically spin coating 50 μL of polymer at 500 rpm for 10 s then 600 rpm for

30 s. All degassed solutions were spin coated in an N_2 filled glove box and ambient solutions were spin coated in air. The 1,2-dichlorobenzene OECTs were spin coated onto the OECT substrates at at 500 rpm for 10 s then 600 rpm for 30 s and then annealed at 40ºC hotplate for 30 minutes before testing.

Polymer solution preperation. p(g3T2) and p(g2T2-g4T2) were synthesized according to [66] and used as received. pgBTTT was synthesized according to [90] and used as received. All ambient polymer solutions were prepared in air using solvents stored in air as received. Ambient-chloroform p(g3T2), p(g2T2-g4T2), and pgBTTT solutions were prepared in solvent blend with a volume ratio of 20 % volume fraction chlorobenzene to 80 % volume fraction chloroform at a 5mg/mL concentration. Ambient-1,2-dichlorobenzene p(g3T2) polymer solution was prepared in a solvent blend with a volume ratio of 20 % volume fraction chlorobenzene to 80 % volume fraction 1,2-dichlorobenzene at a 5mg/mL concentration. Non-anhydrous, amylene stabilized chloroform was used and purchased from Electron Microscopy Sciences. Anhydrous chlorobenzene was purchased from J.T.Baker and 1,2-dichlorobenzene used was purchased from Sigma-Aldrich. All solvents were filtered with a PTFE membrane syringe filter of 0.45 μm pore size. The same solvents were then degassed using the freeze-pump-thaw method, sealed, and stored in an N_2 filled glove box. Degassed-chloroform p(g3T2), p(g2T2-g4T2), and pgBTTT solutions were prepared in an N_2 filled glove box with the same solvent ratios as before using degassed solvents. Degassed 1,2-dichlorobenzene p(g3T2) polymer solution was prepared using the same solvent ratios as before with degassed solvents in an N_2 filled glove box. Degassed $C_{60}F_{48}$ and BCF dopant solutions were prepared using the same degassed chlorobenzene in an N_2 filled glove box at varying concentrations. The degassed $C_{60}F_{48}$ dopant solution was admixed with a 5 mg/mL solution of p(g3T2) and p(g2t2-g4T2) consisting of the same degassed chloroform to form a p(g3T2):$C_{60}F_{48}$ solution containing 80% chloroform and 20 % volume fraction chlorobenzene. The p(g3T2):$C_{60}F_{48}$ doped solutions were prepared in (0, 50, 100, 300, and 600) mol% concentrations using the same methods as previously reported so that effects from solvent interactions are normalized for every solution.[88,95,71,63,86,88] Mol% is calculated as a molar percentage of the total molar mass of the polymer, calculated from the average molecular weight. p(g2T2-g4T2): $C_{60}F_{48}$ doped solutions were prepared on (0, 20, 50, and 100) mol% concentrations. A degassed p(g3T2):$C_{60}F_{48}$ doped solution was prepared with solvent ratio containing 80 %

volume fraction 1,2-dichlorobenzene and 20 % volume fraction $C_{60}F_{48}$ chlorobenzene solution in an N_2 filled glove box. A degassed pgBTTT:BCF solution was prepared in an N_2 filled glove box with degassed chloroform and 20 % volume fraction chlorobenzene BCF dopant solution. Each solution was allowed to rest overnight before spin coating. All solutions were prepared on the same day from the same polymer batch for each polymer:dopant sample set.

Organic electrochemical transistor characterization and analysis. The majority of this manuscript – apart from the final section and stability tests – test the devices in an inert environment, by using an N_2 filled glove box and $[BMIM]BF_4$ as an ionic liquid electrolyte. This was to remove any impact from oxygen. A bottom-gate bottom-contact transistor architecture was used for the $[BMIM]BF_4$ electrolyte, that used a 500×500 μm gold patterned electrode coated with p(g3T2) as the gate. All current-voltage characteristics were measured using a Keysight B2912A Precision Source/Measure Unit. The scan rate for all the transfer data is 0.52 V/s with V_G= 0.2V to -0.8V and V_D:-0.05V, -0.6V. The scan rate for the output curves is 0.28 V/s with V_D= 0 V to -0.6 V and V_G = 0 V to V_G = -0.8 V, with a step of ΔV_G = 0.12 V. All comparative transfer and output currents were normalized according to film thicknesses to account for the effects of film thickness. OECTs tested in non-inert environments were tested outside the glovebox and used an aqueous electrolyte, 0.1 mol/L $NaCl_{aq}$, in a top-gate bottom-contact architecture, that used a Ag/AgCl pellet as the gate electrode. All OECTs were prepared on the same day for each polymer:dopant sample set. Stability tests were carried out in the ambient testing setup, and used a wax-sealed polydimethylsiloxane (PDMS) well to prevent the 0.1M NaCl aqueous electrolyte from evaporating during the test windows.

Electrochemical Impedance Spectroscopy and Capacitance Voltage. Cyclic voltammetry was taken using an Autolab potentiostat in air at a rate of 0.05 V/s for 3 cycles. Electrochemical impedance spectroscopy (EIS) was used to determine the volumetric capacitance for all devices where $[BMIM]BF_4$ ionic liquid was used as the electrolyte solution, a platinum (Pt) wire served as the counter electrode, and two 500x500 μm gold (Au) patterned electrodes coated with p(g3T2) were used as the working and reference electrodes. Afterwards, CV and EIS scans were taken again using aqueous 0.1 mol/L NaCl electrolyte and Pt wire as the counter electrode. The same 500×500 μm Au electrode coated with p(g3T2) was used as the working electrode and an Ag/AgCl

pellet was used as the reference electrode. EIS measurements were taken at 10 mV sine wave at frequencies ranging from 1 $\times 10^5$ Hz to 0.1 Hz and a DC offset potential at the max V_{Gm} for the polymer thin film. The data analysis was done using Metrohm Autolab NOVA software. We note that the EIS set ups are different for the two electrolytes, i.e., [BMIM]BF_4 and $NaCl_{aq}$. The set ups use different counter electrode materials (AgAgCl and polymer coated Au, for the $NaCl_{aq.}$ and BMIM]BF_4, respectively), and position of the counter electrode in the EIS set up is different. The position is different because of the different OECT architectures: bottom-contact top-gate for the $NaCl_{aq.}$ and bottom-contact bottom-gate for the [BMIM]BF_4.

Thickness measurements. A Dektak Profilometer was used to measure film thickness of the polymer thin-films as cast in the OECT channels and on the gate electrode. Thickness value was determined by taking the average from five thickness measurements.

Ultraviolet photoelectron spectroscopy. A thin film of p(g3T2) processed from degassed-CF and a thin-film p(g3T2):$C_{60}F_{48}$ were formed by spin coating 5mg/mL polymer in an N_2 environment on clean ITO substrates at 1800 rpm for 30 s. Another p(g3T2) thin film was prepared in the same way using ambient solvents and spin cast in air. UPS measurements were performed using a PHI 5600 UHV system coupled with a hemispherical electron energy analyzer and a multichannel detector with a 5.85 eV pass energy. An Excitech H Lyman-α lamp (E-lux 121, 10.2 eV emission) was used as the photon source with a 90° mirror (E-lux EEM Optical Module) and a dry oxygen purge through the beam path at between 933 Pa and 1333 10 Pa. A negative 5 V bias was applied to the samples during the measurements.

Electron Paramagnetic Resonance. EPR polymer solution samples were prepared at a concentration of 10mg/mL of p(g3T2) polymer with a solvent solution containing 80 % volume fraction degassed chloroform and 20 % volume fraction degassed chlorobenzene in an N_2 filled glove box. A capillary tube was filled with the degassed solution and sealed airtight in an N_2 filled glove box before testing. An ambient p(g3T2) polymer solution was prepared using ambient chloroform and chlorobenzene in the same solvent ratios in air. A capillary tube was filled with the ambient p(g3T2) solution and sealed in air before testing. Both capillaries were filled with identical volume. Another set of chloroform p(g3T2) solutions were prepared at a concentration

of 5 mg/mL containing 80 % volume fraction chloroform and 20 % volume fraction chlorobenzene with ambient solvents and doped p(g3T2):$C_{60}F_{48}$ (100 mol%) solution was prepared in the same way but using 20 % volume fraction of a $C_{60}F_{48}$ degassed chlorobenzene solution. A third capillary tube was filled with the same $C_{60}F_{48}$ solution used to dope the 100 mol% p(g3T2):$C_{60}F_{48}$ solution. The EPR spectra was recorded using a Bruker EMX PremiumX at room temperature, with 15 dB microwave attenuation, 100 kHz modulation frequency, and a modulation amplitude of 1.00 G. EPR measurements were carried out at room temperature, with identical sample volume and measurement conditions.

Atomic force microscopy. Topographical information and surface roughness measurements were taken using a Cypher S atomic force microscope operating in tapping mode on p(g3T2) thin films prepared in the same method as described for UV-vis. Data analysis was carried out using Igor Pro.

Grazing Incidence Wide Angle X-ray. Films of each polymer we prepared as described above on silicon oxide coated silicon substrates. The GIWAXS data was collected at the 11-BM CMS beamline of NSLS-II in a vacuum environment using a Pilatus 900 k detector and a photon energy of 13.5 keV. The sample detector distance was nominally 260 m, and the angle of incidence was varied between 0.1 and 0.14 degrees relative to the substrate. Analysis was performed using the Nika software package for wavemetrics Igor Pro.

Fourier Transform Infrared Spectroscopy. Theoretical IR vibrational spectra were calculated using frequency calculations on optimized structures at B3LYP/6-31G* level in the gas phase, using a scaling factor of 0.96 based on data from NIST (https://cccbdb.nist.gov/vibscalejust.asp). Spectra were produced using GaussSum software [96] with line broadening of full width at half maximum (FWHM) 10 cm^{-1}. Vibrational modes were visualized with the Jmol software.

Ultraviolet photoelectron spectroscopy on 5,11-bis(triethylsilylethynyl)anthradithiophene (TES-ADT). Experiments demonstrating oxygen is present in the ambient-CF, but not present in the degassed-CF. We prepared two chloroform solutions with TES-ADT of the same concentration. One solution was prepared in a N_2 filled glove box using degassed chloroform and

sealed in an airtight UV-transparent cuvette and the other solution was prepared in air using ambient chloroform and sealed in another UV-transparent cuvette. The initial UV spectra of the degassed-TES-ADT and ambient-TES-ADT solutions were first matched to ensure identical initial concentration. The cuvettes were then subject to incandescent light for 1-minute increments. UV spectra were acquired after every minute of light exposure. Both cuvettes were placed at equal distance from the light source. A dual fiber optic illuminator was used to ensure even light irradiation to the samples. UV spectra was acquired using an Agilent Cary 60 UV-Vis spectrophotometer from 300 nm to 700 nm. A background spectrum acquired from a cuvette with ambient chloroform was recorded for baseline correction.

Tables

p(g3T2) OECT metrics: Average values taken from six OECTs								
Test conditions		**g_m (mS)**	**$\mu_{gm}C^*$ (F/cmVs)**	**$\mu_{transient}$ (cm^2/Vs) [a]**	**C* (F/cm^3) [a]**	**$\mu_{transient}C^*$ (F/cmVs) [a]**	**V_T (V)**	**I_{ON} (A)**
[BMIM][BF_4] electrolyte, tested in inside a nitrogen glovebox	Degassed-CF	0.6 ±0.4	93 ±9	N/A	615	N/A	-0.13 ±0.01	8.1×10^{-5}
	Ambient-CF	2.9 ±1.4	113 ±6	0.01	528	5.8	-0.12 ±0.04	1.2×10^{-3}
	Degassed-CF:$C_{60}F_{48}$(100 mol%)	12.2 ±6.9	680 ±39	0.08	524	43.6	-0.08 ±0.04	5.8×10^{-3}
0.1 mol/L $NaCl_{aq.}$ electrolyte, tested outside the glovebox.	Degassed-CF	5.3 ±1.6	203.6 ±75	N/A	639	N/A	-0.013 ±0.01	1.9×10^{-3}
	Ambient-CF	8.6 ±1.2	281.02 ±52	0.16	581	98.2	-0.015 ±0.01	4.1×10^{-3}
	Degassed-CF:$C_{60}F_{48}$(100 mol%)	18.4 ±4.4	1160.3 ±285	0.20	654	129.6	-0.03 ±0.04	6.4×10^{-3}

[a] Not average values.

Table 1. Summary of the impact of degassed-CF, ambient-CF, and chemically p-doped p(g3T2), i.e., degassed-CF:$C_{60}F_{48}$(100 mol%), on p(g3T2) OECT performance. Mobility (μ) was measured using the OECT transient response ($\mu_{transient}$) outlined in.[97] Based on difficulties using the transient method to calculate $\mu_{transient}$ for degassed-CF systems – most likely because degassed-CF μ is too low for this technique[98] – the μC* product has been calculated in two different ways. First, by multiplying $\mu_{transient}$ with C*. C* was measured using EIS as described in the Experimental Section, and is not an average value. Second, by extracting the μC* product from the peak in g_m[99]. Both show the same trends, i.e., that the μC* product is always greatest in p(g3T2) OECTs processed from degassed-CF:$C_{60}F_{48}$(100 mol%). V_T is extracted from the square root of the drain current vs. the gate voltage. Average values in the table are taken from 6 OECTs per system. All OECTs have channel length and width 50 μm and 500 μm, respectively. The first column in the table indicates whether

[BMIM][BF_4] or 0.1 mol/L $NaCl_{aq}$. If [BMIM][BF_4] is the electrolyte, the OECTS are in a bottom-gate bottom-contact configuration, with a p(g3T2) coated 500×500 µm gold electrode as the gate electrode. If 0.1 mol/L $NaCl_{aq.}$ is the electrolyte, the OECTS are in a top-gate bottom-contact configuration, with a silver-silver chloride pellet as the gate electrode.

System	AFM		GIWAXS: Out of plane				
	RMS (nm)	Film thickness (nm)	Peak (100) q (A^{-1})	Error	Real space (A)	% change relative to degassed	Film thickness (nm)
Ambient-CF	14.8 ±2.3	71.7 ±6.2	0.3212	0.0003	19.56	3.9	108 nm
Degassed-CF	18.5 ±2.8	72.4 ±6.1	0.3342	0.0003	18.80	0	101
p(g3T2):$C_{60}F_{48}$(100 mol%)	2.2 ±0.4	39.2 ±2.8	0.3204	0.0006	19.61	4.1	33

Table 2. OECT channel thin film thickness as measured with Dektak and AFM root mean squared surface roughness. GIWAXS out of plane q values. Film thickness values are average values from five thickness measurements.

Polymer	g_m (mS)	$I_{ON/OFF}$	W (µm)	L (µm)	d (nm)	Architecture	V_D	µ (cm^2/Vs)	µ extraction method	Electrolyte	V_T	Ref.
gDPP-g2T	203.5 ± 34.4	3.3×10^5	30	30	100	vOECT	-0.5	$(3.33 \pm 0.3) \times 10^{-3}$	transient time	PBS	N/A	25
PEDOT:PSS	4.02		10	10	100	planar	-0.6			NaCl		100
p(g3T2)	8.9 ± 1	10^5	100	10	75	planar	-0.6	0.90 ± 0.10	slope g_m	NaCl	0.03	66
p(g2T2-g4T2)	6.5 ± 1.6	10^5	100	10	45	planar	-0.6	1.72 ± 0.31	slope g_m	NaCl	0.02	66
p(gPyDPP-MeOT2)	--	10^5	100	10	60	planar	-0.4	0.030 ± 0.007	transient time	NaCl	--	42
crystallized pedot:pss	18.5	--	80	20	0.2	planar	-0.6	--	--	--	--	101

PEDOT:PSS	32	--	500	5	0.2	internal ion gate - planar	-0.6	--	--	--	--	[102]
PEDOT:PSS	63.45 ± 5	10^4	50	0.15	50	ultra - short channel	-0.5	N/A	N/A	[Li+ TFSI−]	N/A	[103]
p(g2T-T)	21	4×10^5	100	10	160	planar	-0.4	0.28	N/A	NaCl	0.15	[74]
pBTTT	21.0 ± 0.7	10^5	N/A	N/A	108	planar	-0.6	3.44 ± 0.13	$\sqrt{I_D}$	NaCl	−0.24	[90]
p(g2T-TT)	6.2 ± 0.6	10^5	N/A	N/A	111	planar	-0.6	0.41 ± 0.14	$\sqrt{I_D}$	NaCl	0.01	[90]
p(g3T2):$C_{60}F_{48}$	25.1	1.4×10^6	500	50	39	planar	-0.6	3.32	max g_m	[BMIM][BF_4]	-0.08	This work
p(g3T2):$C_{60}F_{48}$	12.5	1.1×10^5	500	50	39	planar	-0.6	1.03	max g_m	NaCl	0.03	This work

Table 3. Summary of accumulation mode p-type OECT performance metrics compared to this work

Supplementary Files

This is a list of supplementary files associated with this preprint. Click to download.

- 4324SupportingInformation.pdf